Clim. Past Discuss., 9, 3209–3238, 2013
www.clim-past-discuss.net/9/3209/2013/
doi:10.5194/cpd-9-3209-2013
© Author(s) 2013. CC Attribution 3.0 License.

Climate of the Past Discussions
Open Access

This discussion paper is/has been under review for the journal Climate of the Past (CP).
Please refer to the corresponding final paper in CP if available.

Salinity changes in the Agulhas leakage area recorded by stable hydrogen isotopes of C_{37} alkenones during Termination I and II

S. Kasper[1], M. T. J. van der Meer[1], A. Mets[1], R. Zahn[2], J. S. Sinninghe Damsté[1], and S. Schouten[1]

[1]NIOZ Royal Netherlands Institute for Sea Research, Department of Marine Organic Biogeochemistry, P.O. Box 59, 1790 AB Den Burg (Texel), the Netherlands
[2]Universitat Autònoma de Barcelona, Institut de Ciència i Tecnologia Ambientals, 08193 Bellaterra, Spain

Received: 13 May 2013 – Accepted: 29 May 2013 – Published: 18 June 2013

Correspondence to: S. Kasper (sebastian.kasper@nioz.nl)

Published by Copernicus Publications on behalf of the European Geosciences Union.

Abstract

At the southern tip of the African shelf, the Agulhas Current reflects back into the Indian Ocean causing so called “Agulhas rings” to spin off and release relatively warm and saline water into the South Atlantic Ocean. Previous reconstructions of the dynamics of the Agulhas current, based on paleo sea surface temperature and sea surface salinity proxies, inferred that Agulhas leakage from the Indian Ocean to the South Atlantic is reduced as a consequence of changes in wind fields related to a northwards migration of ice masses and the subtropical front during glacial stages. Subsequently, this might have led to a build-up of warm saline water in the southern Indian Ocean. To investigate this latter hypothesis, we reconstructed sea surface salinity changes using alkenone δD, and paleo sea surface temperature using TEX_{86}^{H} and $U_{37}^{K'}$, from two sediment cores (MD02-2594, MD96-2080) located in the Agulhas leakage area during Termination I and II. Both $U_{37}^{K'}$ and TEX_{86}^{H} temperature reconstructions infer an abrupt warming during the glacial terminations, which is different from the gradual warming trend previously reconstructed based on Mg/Ca ratios of *Globigerina bulloides*. These differences in temperature reconstructions might be related to differences in the growth season or depth habitat between organisms. A shift to more negative $\delta D_{alkenone}$ values of approximately 14 ‰ during glacial Termination I and approximately 13 ‰ during Termination II is also observed. Approximately half of these shifts can be attributed to the change in global ice volume, while the residual isotopic shift is attributed to changes in salinity, suggesting relatively high salinities at the core sites during glacials, with subsequent freshening during glacial terminations. Approximate estimations suggest that $\delta D_{alkenone}$ represents a salinity change of ca. 1.7–2 during Termination I and ca. 1.5–1.7 during Termination II. These estimations are in good agreement with the proposed changes in salinity derived from previously reported combined planktonic foraminifera $\delta^{18}O$ values and Mg/Ca-based temperature reconstructions. Our results show that the δD of alkenones is a potentially suitable tool to reconstruct salinity changes independent of planktonic foraminifera $\delta^{18}O$.

CPD
9, 3209–3238, 2013

1 Introduction

Approximately 2–15 Sv of warm and saline Indian Ocean water is annually released into the South Atlantic Ocean by the Agulhas Current, an ocean current system that is confined by the Subtropical front and the Southern African Coast (Lutjeharms, 2006). The Agulhas Current is fed by warm, saline Indian Ocean water from two sources; the Mozambique Channel, between Madagascar and the East African Coast, and the East Madagascar Current, which merges with the Mozambique Channel flow at approximately 28° S (Penven et al., 2006). When this warm, saline water reaches the Agulhas corridor, the vast majority is transported back into the Indian Ocean via the Agulhas Return Current (Fig. 1). However, between 5 and 7 rings of warm, saline water are released into the Atlantic Ocean per year, termed Agulhas Leakage (Lutjeharms, 2006). These Agulhas rings of Indian Ocean waters have been shown to play an important role in the heat and salt budget in the Atlantic Ocean, thereby impacting the Atlantic Meridional Overturning Circulation (AMOC) (Bard and Rickaby, 2009; Haarsma et al., 2011) and the global Thermohaline Circulation (THC) (Peeters et al., 2004; Biastoch et al., 2008; van Sebille et al., 2011).

The magnitude of Agulhas Leakage into the Atlantic Ocean depends on the strength of the Agulhas Current as well as the position of the retroflection (Lutjeharms, 2006). However, the effect of Agulhas Current strength on the Agulhas leakage efficiency is still debated. For instance, Rouault et al. (2009) suggested that, based on recent temperature observations and modeling experiments, increased Agulhas leakage of warm and saline waters into the South Atlantic Ocean can be associated with increased Agulhas Current transport, while modeling experiments performed by van Sebille et al. (2009) suggested increased Agulhas leakage to be associated with a weakened Agulhas Current.

Previous studies have shown that during glacial stages a weakened and more variable Agulhas Current occurs together with reduced Agulhas Leakage (Peeters et al., 2004; Franzese et al., 2006). Peeters et al. (2004) provide planktonic foraminifera as-

CPD
9, 3209–3238, 2013

semblage data from the Cape Basin record specific to Agulhas leakage waters. They found relatively low contributions of "Agulhas leakage fauna" in the Cape Basin, suggesting a reduced Agulhas Leakage during glacial stages (Rau et al., 2002; Peeters et al., 2004), coinciding with low sea surface temperatures. This suggests a restriction in the Agulhas leakage during cold periods (Peeters et al., 2004). Furthermore, stable carbon isotope gradients have been applied in combination with sea surface temperature reconstructions as indicators for deep-water ventilation efficiency between Atlantic and Pacific Ocean sites further north of the East African coast (Bard and Rickaby, 2009). Results demonstrate a northward migration of the subtropical front during glacial periods (Bard and Rickaby, 2009).

A northward shift of the Subtropical Front and eastward forcing of the retroflection during glacial periods may have led to an increased back transport of warm, saline water into the Indian Ocean during glacial periods (Peeters et al., 2004). Martinez-Mendez et al. (2010) showed increased sea water oxygen isotopes ($\delta^{18}O_{sw}$) values, derived from paired planktonic foraminifera $\delta^{18}O$ and Mg/Ca analysis of *Globigerina bulloides*, in the Agulhas leakage area throughout marine isotope stage 6 (MIS6) and marine isotope stage 3 (MIS3) and early marine isotope stage 2 (MIS2). These elevated $\delta^{18}O_{sw}$ values are likely indicative for increased salinity (Martinez-Mendez et al., 2010). However, it should be noted that salinity reconstructions, based on planktonic foraminifera $\delta^{18}O_{sw}$ values, carry some uncertainties that are difficult to constrain, e.g. assumed constancy for the transfer functions of $\delta^{18}O_{sw}$ to salinity over space and time (Rohling and Bigg, 1998; Rohling, 2000).

Martinez-Mendez et al. (2010) further reported that reconstructed SST, derived from the planktonic foraminifera Mg/Ca of *G. bulloides*, displayed a gradual warming trend starting in the early MIS6 and MIS2 (Martinez-Mendez et al., 2010). This is, however, in contradiction with temperature reconstructions based on $U^{K'}_{37}$ paleothermometry (Peeters et al., 2004; Martinez-Mendez et al., 2010), which showed cooler sea surface temperatures during glacial periods, followed by a rapid warming at the onset of the interglacial stages. These differences may be related to uncertainties associ-

CPD
9, 3209–3238, 2013

ated with the different temperature proxies, i.e. different source organisms. Planktonic foraminiferal Mg/Ca ratios have been shown to not only reflect temperature, but also salinity (Ferguson et al., 2008; Arbuszewski et al., 2010). This has been demonstrated in high salinity environments such as the Mediterranean Sea (Ferguson et al., 2008), and in open ocean settings such as the tropical Atlantic ocean (Arbuszewski et al., 2010). Furthermore, $U^{K'}_{37}$–SST relationships are derived from organisms with different growth seasons and (depth) habitats than the planktonic foraminifera *G. bulloides*, potentially recording different temperature ranges.

In this study, we provide salinity and temperature proxies to investigate salinity changes in the Agulhas leakage area, as well as discussing the divergent behavior of the Mg/Ca and $U^{K'}_{37}$ temperature proxies. We used the hydrogen isotope composition of the combined $C_{37:2-3}$ alkenones ($\delta D_{alkenone}$), produced by haptophyte algae, as a proxy for relative changes in sea surface salinity (SSS). Culture experiments for two common open ocean haptophyte species, *Emiliania huxleyi* and *Gephyrocapsa oceanic*, have shown that the hydrogen isotope composition of alkenones is mainly dependent on (1) salinity and (2) the hydrogen isotope composition of the growth media, and to a lesser extent (3) growth rates (Schouten et al., 2006). Application of the hydrogen isotope composition of alkenones has resulted in reasonable salinity reconstructions for the eastern Mediterranean and Black Sea (van der Meer et al., 2007, 2008). Here, we apply the $\delta D_{alkenone}$ to estimate relative salinities of the Agulhas system focusing on Termination I and Termination II using the same cores used by Martinez-Mendez et al. (2010), situated in the Agulhas Leakage area, off the coast of South Africa (Fig. 1). In order to assess the effect of growth rates on $\delta D_{alkenone}$, we measure the stable carbon isotope composition of the combined $C_{37:2-3}$ alkenones ($\delta^{13}C_{alkenones}$) on samples from glacials and interglacials (Rau et al., 1996; Bidigare et al., 1997; Schouten et al., 2006). Furthermore, we reconstruct SST using the TEX^{H}_{86} proxy (Schouten et al., 2002; Kim et al., 2010) and compare this with the $U^{K'}_{37}$ and

CPD
9, 3209–3238, 2013

Mg/Ca record of the planktonic foraminifera *G. bulloides* for the same sediment cores (Martinez-Mendez et al., 2010).

2 Material and methods

2.1 Setting

Sediment samples were taken from cores MD96-2080 (36° 19.2′ S; 19° 28.2′ E, 2488 m water depth) and MD02-2594 (34° ,42.6′ S; 17° 20.3′ E, 2440 m water depth) off the coast of South Africa (Fig. 1). Core MD02-2594 was taken during the RV *Marion Dufresne* cruise MD128 "SWAF" (Giraudeau et al., 2003). Core MD96-2080 was obtained during the IMAGES II Campaign "NAUSICAA" (Bertrand et al., 1997). Age models and records of *Globigerina bulloides* δ^{18}O and Mg/Ca have previously been established for both sediment cores (Martinez-Mendez et al., 2008, 2010). The sampled interval of core MD02-2594 covered the period 3 to 42 ka (MIS1 to mid MIS3) and included Termination I. Core MD96-2080 covered the period between 117–182 ka (MIS5e to MIS6) and included Termination II (Tables 1, 2).

2.2 Sample preparation

Sediment samples were freeze dried and homogenized with a mortar and pestle. The homogenized material was then extracted using the accelerated solvent extractor method (ASE) with dichloromethane (DCM) : methanol 9 : 1 (v/v) and a pressure of 1000 psi in 3 extraction cycles. The total lipid extract was separated over an Al_2O_3 column into a apolar, ketone and polar fraction using hexane : DCM 9 : 1, hexane : DCM 1 : 1 and DCM : methanol 1 : 1, respectively. The ketone fraction was analyzed for $U^{K'}_{37}$ using gas chromatography. Gas chromatography/high-temperature conversion/isotope ratio mass spectrometry (GC/TC/irMS) was used to measure the combined hydrogen isotope composition of the di- and tri-unsaturated C_{37} alkenones. The polar fraction

CPD
9, 3209–3238, 2013

was analyzed for TEX_{86}^{H} using high performance liquid chromatography mass spectrometry (HPLC/MS). Stable carbon isotopes of the combined di- and tri-unsaturated C_{37} alkenones were analyzed using GC/combustion/irMS.

2.3 $U_{37}^{K'}$ analysis

Ketone fractions were analyzed by gas chromatography (GC) using an Agilent 6890 gas chromatograph with a flame ionization detector and a Agilent CP Sil-5 fused silica capillary column (50 m × 0.32 mm, film thickness = 0.12 µm) with helium as the carrier gas. The GC-oven was programmed to subsequently increase the temperature from 70 to 130 °C with 20 °C min^{-1} steps, and then with 4 °C min^{-1} steps to 320 °C, at which it was held isothermal for 10 min. $U_{37}^{K'}$ values were calculated according to Prahl and Wakeham (1987). Subsequently, SST was calculated using the core top calibration established by Müller et al. (1998).

2.4 δD of alkenone analysis

Alkenone hydrogen isotope analyses were carried out on a Thermo-Finnigan DELTA^{Plus} XL GC/TC/irMS. The temperature conditions of the GC increased from 70 to 145 °C with 20 °C min^{-1} steps, then to 320 °C with 4 °C min^{-1} steps, at which it was held isothermal for 13 min using an Agilent CP Sil-5 column (25 m × 0.32 mm) with a film thickness of 0.4 µm and 1 mL min^{-1} helium at constant flow. The thermal conversion temperature was set to 1425 °C. The H_3^+ correction factor was determined daily and ranged between 10 and 14. Isotopic values for alkenones were standardized against pulses of H_2 reference gas, which was injected three times at the beginning and two times at the end of each run. A set of standard *n*-alkanes with known isotopic composition (Mixture B prepared by Arndt Schimmelmann, University of Indiana) was analyzed daily prior to each sample batch in order to monitor the systems performance. Samples were only analyzed when the alkanes in Mix B had an average deviation from their off-line determined value of < 5 ‰. Squalane was co-injected as an internal standard with

CPD
9, 3209–3238, 2013

each sample to monitor the precision of the alkenone isotope values. The squalane standard yielded an average δD-value of $-167\,‰ \pm 4.5$, which compared favorably with its offline determined δD-value of $-170\,‰$. Alkenone δD values were measured as the combined peak of the $C_{37:2}$ and $C_{37:3}$ alkenones (van der Meer et al., 2013) and fractions were analyzed in duplicates if a sufficient amount of sample material was available. Standard deviations of replicate analyses varied from ±0.1 ‰ to ±5.9 ‰.

2.5 δ^{13}C of alkenone analyses

Combined $C_{37:2-3}$ alkenones were analyzed using a Thermo Delta V isotope ratio monitoring mass spectrometer coupled to an Agilent 6890 GC. Samples were dissolved in hexane and analyzed using a GC temperature program starting at 70 °C, then increasing to 130 °C at 20 °C min^{-1} steps, and then to 320 °C at 4 °C min^{-1} steps, where it was held for 20 min. The stable carbon isotope compositions for $\delta^{13}C_{alkenone}$ are reported relative to Vienna Pee Dee Belemnite (VDPB). The $\delta^{13}C_{alkenone}$ values are averages of at least two runs. GC-irMS performance was checked daily by analyzing a standard mixture of n-alkanes and fatty acids, including two fully perdeuterated alkanes with a known isotopic composition. These perdeuterated alkanes were also co-injected with every sample analysis and yielded an average δ^{13}C value of -32.5 ± 0.5 ‰ and -27.0 ± 0.5 ‰ for *n*-C_{20} and *n*-C_{24}, respectively. This compared favorably with their offline determined δ^{13}C-values of −32.7 ‰ and −27.0 ‰ for *n*-C_{20} and *n*-C_{24}, respectively.

2.6 TEX_{86}^{H} analysis

Analyses for TEX_{86}^{H} were performed as described by Schouten et al. (2007). In summary, an Agilent 1100 series HPLC/MS equipped with an auto-injector and Agilent Chemstation chromatography manager software was used. Separation was achieved on an Alltech Prevail Cyano column (2.1 mm × 150 mm, 3 µm), maintained at 30 °C. Glycerol dibiphytanyl glycerol tetraethers (GDGTs) were eluted with 99 % hexane and

CPD
9, 3209–3238, 2013

1 % propanol for 5 min, followed by a linear gradient to 1.8 % propanol in 45 min. Flow rate was 0.2 mL min^{-1} by back-flushing hexane/propanol (90 : 10, v/v) at 0.2 mL min^{-1} for 10 min. Detection was achieved using atmospheric pressure positive ion chemical ionization mass spectrometry (APCI-MS) of the eluent. Conditions for the Agilent 1100 APCI-MS were as follows: nebulizer pressure of 60 psi, vaporizer temperature of 400 °C, drying gas (N_2) flow of 6 L min^{-1} and temperature 200 °C, capillary voltage of −3 kV and a corona of 5 µA (~ 3.2 kV). GDGTs were detected by Single Ion Monitoring (SIM) of their $[M+H]^+$ ions (dwell time = 234 ms) (Schouten et al., 2007a) and quantified by integration of the peak areas. The TEX_{86}^H values were calculated according to Kim et al. (2010). The TEX_{86}^H–SST calibration model by Kim et al. (2010) was used to transfer TEX_{86}^H-values to absolute SST. This calibration model is recommended for temperature reconstruction above 15 °C (Kim et al., 2010) and therefore appears to be the most suitable model for reconstructing subtropical temperatures, as found in the Agulhas leakage area.

3 Results

3.1 Sea surface temperature proxies

The $U_{37}^{K'}$ record of MD96-2080 indicated constant temperatures of approximately 20.7 ± 0.5 °C throughout MIS6 (138–182 ka) (Table 1, Fig. 2). With the onset of Termination II at approximately 138 ka, temperatures began to increase to a maximum of ~ 25 °C during early MIS5e (~ 125 ka), followed by a slight decrease in temperature towards ~ 23 °C at about 120 ka. The $U_{37}^{K'}$ SST record for MD02-2594 indicated relatively constant temperatures of 20 ± 0.5 °C throughout MIS3 and early MIS2 (Table 2, Fig. 3). With the onset of Termination I during mid-MIS2 (~ 18 ka), temperatures showed a slight warming towards ~ 22 °C at the beginning of MIS1. Throughout MIS1, temperatures slightly decreased to approximately 21 °C.

CPD
9, 3209–3238, 2013

The overall pattern in the TEX_{86}^{H} records for the two cores indicated that absolute temperatures were cooler by up to 5 °C compared to $U_{37}^{K'}$ temperatures during glacial and interglacial stages MIS5e and MIS6, as well as MIS3/MIS2 and MIS1. During MIS6, TEX_{86}^{H} temperatures were relatively stable at 17 ± 1 °C, although less stable than $U_{37}^{K'}$ SST (Table 1, Fig. 2). At the initial termination of the glacial MIS6 (ca. 135–138 ka), reconstructed TEX_{86}^{H} temperatures increased rapidly to about 22 °C, which is similar in absolute terms compared to $U_{37}^{K'}$ SST (Fig. 2). Subsequently, TEX_{86}^{H} SST decreased rapidly to ~ 20 °C and remained constant during MIS5e. During MIS3 and early MIS2, TEX_{86}^{H} SST showed a trend towards cooler temperatures from approximately 17 °C at ~ 38 ka to 14 °C at the start of Termination I (18 ka) (Table 2, Fig. 3). At the onset of Termination I, TEX_{86}^{H} SSTs abruptly increased. Temperatures reached a maximum of 19 °C at the beginning of MIS1 (11 ka) and decreased again to relatively constant temperatures of ca. 18 °C throughout MIS1. This trend is comparable to the $U_{37}^{K'}$ SST record, albeit with a negative offset of approximately 4 °C throughout MIS3/MIS2 and MIS1, and approximately 2 °C during the glacial termination phase (11–18 ka) (Fig. 3).

3.2 Stable hydrogen and carbon isotope composition of $C_{37:2-3}$ alkenones

The $\delta D_{alkenone}$ values in core MD96-2080 ranged between −177 to −198 ‰ (Table 1). During early MIS6 (169 to 181 ka), $\delta D_{alkenone}$ values were approximately −189 ± 2 ‰ and shifted to more positive values of ca. −177 ‰ at 158 ka. In the time interval between 142 to 162 ka (MIS6), $\delta D_{alkenone}$ decreased to −180 ± 3 ‰. During glacial Termination II (130 to 138 ka) the $\delta D_{alkenone}$ values decreased abruptly to approximately −194 ± 3 ‰ for MIS5e (118–130 ka) (Fig. 2). The $\delta D_{alkenone}$ values in core MD02-2594 ranged between −166 to −192 ‰ (Table 2). In the time interval from 12 to 41 ka (MIS3 and MIS2), values for $\delta D_{alkenone}$ were relatively constant at approximately −175 ± 4 ‰ (Fig. 3). At ca. 11 ka (onset of MIS1), $\delta D_{alkenone}$ values shifted to more negative values with an average of −188 ± 5 ‰ for the time period of 3 to 9 ka (MIS1) (Fig. 3).

CPD
9, 3209–3238, 2013

The stable carbon isotope composition of the alkenones ($\delta^{13}C_{alkenone}$) was analyzed from selected sediment samples before, within and after each glacial termination stage (Tables 1 and 2). In the time period before the termination phase of glacial MIS6 (141–152 ka) the alkenones had an average $\delta^{13}C$ value of -24.9 ± 0.3 ‰. Within the termination phase (133–138 ka), $\delta^{13}C_{alkenone}$ values are were slightly more enriched in ^{13}C, i.e. -24.2 ± 0.3 ‰. During MIS5e, $\delta^{13}C_{alkenone}$ values became more negative and were on average -25.3 ± 0.4 ‰ (Table 1). For core MD02-2594, the $\delta^{13}C_{alkenone}$ values were fairly constant between −23.6 to −24.1 ‰ (Table 2).

4 Discussion

4.1 Development of sea surface temperatures during Terminations I and II

Application of the $U^{K'}_{37}$ proxy resulted in the highest reconstructed temperatures compared to the TEX^{H}_{86} and Mg/Ca SST reconstructions. The $U^{K'}_{37}$ proxy was approximately 3–4 °C warmer throughout the glacials MIS3 and MIS6 as well as the interglacials MIS1 and MIS5e. However, the TEX^{H}_{86} and planktonic Mg/Ca derived temperatures were only 2 °C less than $U^{K'}_{37}$ SST during the actual glacial terminations (Figs. 2 and 3). The $U^{K'}_{37}$ SST record from this study is in agreement with the $U^{K'}_{37}$ temperature records from the southern Cape Basin (Peeters et al., 2004) and upstream northeast in the Agulhas Current (Bard and Rickaby, 2009) in terms of timing and range of temperature values. This indicates a consistent regional pattern for $U^{K'}_{37}$ temperature records across the wider Agulhas region (Fig. 4).

Reconstructed temperatures based on $U^{K'}_{37}$ yield a core top calibration uncertainty of ±1.5 °C (Müller et al., 1998). For TEX^{H}_{86}, the uncertainty is ±2.5 °C (Kim et al., 2008) and for the culture calibration of SST to Mg/Ca ratios of *G. bulloides*, the uncertainty is ±1.1 °C (Mashiotta et al., 1999). Therefore, absolute temperature differences between

CPD
9, 3209–3238, 2013

proxies of > 3.0 °C are significantly different; i.e. $U^{K'}_{37}$ SST values are significantly higher than TEX^{H}_{86} and Mg/Ca SST for most parts of the records, while the latter two proxies give similar absolute temperature estimates. The difference in absolute temperatures may be explained by a variety of reasons such as growth seasons and/or depth habitats between the alkenone producers, the Thaumarchaeota (Glycerol dialkyl glycerol tetraether (GDGT) producers) and the planktonic foraminifera (Bard, 2001; Lee et al., 2008; Saher et al., 2009; dos Santos et al., 2010; Huguet et al., 2011).

Modern seasonal sea surface temperature variability (< 30 m water depth) varies by up to 5 °C between austral summer (January–March) and austral winter (July–September) in the Agulhas System (Weeks et al., 1998; Locarnini, 2010; Fallet et al., 2011). This temperature difference may explain the offset between $U^{K'}_{37}$ and the other two SST proxies, i.e alkenones produced in the warm season compared to thaumarchaeotal GDGTs and *G. bulloides* carbonate shells in the cool season. Alternatively, the colder temperatures of TEX^{H}_{86} and Mg/Ca may be due to a deeper depth habitat of Thaumarchaeota and *G. bulloides*. Temperatures decrease by 4 °C within the first 100 m in the Agulhas System (Locarnini, 2010; Fallet et al., 2011) and thus Thaumarchaeota and *G. bulloides* could be recording subsurface temperatures. Indeed, it has been shown that Thaumarchaeota inhabit a large depth range in the water column (Karner et al., 2001; Herndl et al., 2005) and that TEX_{86} can reflect subsurface temperatures (Wuchter et al., 2006; Lee et al., 2008; dos Santos et al., 2010). Furthermore, it has been reported that *G. bulloides* has a calcifying depth typically between 50–100 m (Niebler et al., 1999), meaning that reconstructed temperatures based on Mg/Ca may reflect subsurface temperatures rather than actual sea surface temperatures. Conversely, the photosynthesizing alkenone producers are bound to the photic zone and are therefore more likely to reflect ocean surface temperatures (Müller et al., 1998; Fallet et al., 2011).

The timing of the warming trend reflected in the foraminifera Mg/Ca record is different from the $U^{K'}_{37}$ and TEX^{H}_{86} records, as well as other $U^{K'}_{37}$ records in the region (Peeters

CPD
9, 3209–3238, 2013

et al., 2004). The Mg/Ca SST record identifies a warming trend starting in the early glacial periods and gradually extending over the glacial termination phases (Martinez-Mendez et al., 2010). However, the $U^{K'}_{37}$ and TEX^{H}_{86} records show a more abrupt warming at the onset of the glacial terminations (Fig. 4). It has been reported that changes in salinity can affect the Mg/Ca ratios in foraminifera shells, specifically during glacial periods when salinity was likely elevated (Ferguson et al., 2008; Arbuszewski et al., 2010). Thus, the observed trend in Mg/Ca from *G. bulloides* may result from a combined salinity and temperature signal.

Regardless of the cause of the temperature offsets, the overall patterns in $U^{K'}_{37}$ and TEX^{H}_{86} SST suggest cooler conditions throughout stages MIS6 and MIS3/2. This is then followed by an abrupt warming during succeeding glacial terminations, leading to warmer conditions in the interglacial stages MIS5e and MIS1. This pattern fits well with $U^{K'}_{37}$ derived temperature reconstructions from other sediment cores in the area of this study site (Schneider et al., 1995; Peeters et al., 2004; Bard and Rickaby, 2009). The temperature reconstructions based on Mg/Ca and TEX^{H}_{86} show maximum temperatures occurred at the onset of the interglacial MIS5e. However, $U^{K'}_{37}$ temperature reconstructions identified that SST maxima occurred 5 ka later and was only observed in Termination II and not for Termination I. This potentially points towards an increased influence of warm Indian Ocean waters, and hence increased Agulhas Leakage. This in turn is likely related to a southward shift of the sub-tropical front due to shifting wind fields and a southward migration of the land ice shields (Peeters et al., 2004). Nevertheless, these observations do not necessarily imply a buildup of warm Indian Ocean waters prior to glacial terminations at the core site.

4.2 Salinity changes during termination

The $C_{37:2-3}$ alkenone hydrogen isotope records consistently show a substantial decrease toward more deuterium depleted values during the glacial terminations and the interglacial stages MIS5e and MIS1 (Figs. 2 and 3). We quantified changes from glacial

CPD
9, 3209–3238, 2013

to interglacial stages by averaging time intervals from before and after each termination. We observed average shifts in $\delta D_{alkenone}$ of approximately 14 ‰ and 13 ‰ from before to after Termination I and II, respectively (Table 3). These shifts in the $\delta D_{alkenone}$ values can be caused by a number of factors such as: (1) decreasing δD of sea water (δD_{sw}) as an effect of decreasing global ice volume during the terminations (Rohling, 2000), (2) ocean salinity, (3) algal growth rate, and (4) haptophyte species composition (Schouten et al., 2006). We estimate the effect of changes in global ice volume on the $\delta D_{alkenone}$ by using the global mean ocean $\delta^{18}O_{sw}$ record based on benthic foraminifera (Waelbroeck et al., 2002) and calculated a δD_{sw} equivalent by applying a local Indian Ocean meteoric waterline (Srivastava et al., 2010). Changes in δD_{sw} due to the ice volume effect for the selected average intervals before and after the Terminations are estimated to be approximately −6 ‰ during Termination I and II (Table 3). This shift is smaller than that observed in $\delta D_{alkenone}$, suggesting an increase in hydrogen isotopic fractionation during the two Terminations. Based on the culture results of Schouten et al. (2006), this increased fractionation can reflect either changes in growth rate, species composition or salinity.

In order to assess changes in growth rate for the haptophytes, we measured the stable carbon isotope composition of the combined $C_{37:2-3}$ alkenones ($\delta^{13}C_{alkenone}$) (Tables 1 and 2). Our results show relatively small differences in $\delta^{13}C_{alkenone}$ values between glacial and interglacial periods. The fractionation of stable carbon isotopes is mainly controlled by physiological factors like growth rate, cell size and geometry, as well as by the supply of dissolved CO_2 (Rau et al., 1996; Bidigare et al., 1997). The more depleted alkenone $\delta^{13}C$ values during interglacials suggest either slightly higher dissolved CO_2 concentrations or lower growth rates. We suggest that higher dissolved CO_2 concentrations likely explains the more depleted alkenone $\delta^{13}C$ values as CO_2 concentrations were higher during interglacials compared to glacials (Curry and Crowley, 1987). Depleted alkenone $\delta^{13}C$ values may also suggest growth rates were either similar or smaller during interglacials compared to glacials. However, since reduced growth rates would result in decreasing hydrogen isotopic fractionation, our

CPD
9, 3209–3238, 2013

observed increase in hydrogen isotopic fractionation during interglacials compared to glacials cannot be explained by growth rate changes (Schouten et al., 2006).

Assemblage studies in the Agulhas Leakage have shown an increasing abundance of the predominant haptophyte *E. huxleyi* at the beginning of MIS7 towards MIS1, with a maximum relative abundance observed at the onset of MIS1 (Flores et al., 1999). *G. oceanica*, however, reaches maximum relative abundances during Termination II (Flores et al., 1999). Therefore, the effect of changes in the coccolithophore assemblage, toward a dominance of *G. oceanica*, could have a potential bias towards more negative $\delta D_{alkenone}$ values (Schouten et al., 2006). However, the abundance of *G. oceanica* did not exceed the relative abundance of *E. huxleyi* and therefore unlikely had an impact on $\delta D_{alkenone}$ values during Termination II (Flores et al., 1999). In the case of Termination I, the haptophyte *E. huxleyi* reached its maximum relative abundances compared to *G. oceanica*, which showed only minor increases in relative abundance (Flores et al., 1999). This would infer a possible bias towards more positive $\delta D_{alkenone}$ values rather than the observed trend toward more depleted values (Schouten et al., 2006). The observed trends towards more depleted values in the $\delta D_{alkenone}$ during the glacial terminations are therefore not affected to a large extend by changes in the coccolithophore species composition.

Since the residual $\delta D_{alkenone}$ shift, after ice volume correction, of approximately −8 and −7 ‰ for Termination I and II, respectively, cannot be explained by growth rate or species composition changes, we suggest that this residual $\delta D_{alkenone}$ reflects changes in sea surface salinity. We find decreased fractionation during the glacials MIS6 and MIS2/3 subsequently leading to increased fractionation during MIS5e and MIS1, pointing towards a decrease in salinity compared to glacials (Figs. 2 and 3). Indeed, reconstructed $\delta^{18}O_{sw}$ from the planktonic foraminifera *G. bulloides* also indicates higher salinity throughout the glacials MIS6 and MIS3/MIS2 (Figs. 2 and 3) (Martinez-Mendez et al., 2010). However, alkenone δD values begin to shift toward more depleted values shortly before the start of Termination II, at approximately 135 ka, whereas the initial freshening recorded in the $\delta^{18}O_{sw}$ begins at about 133 ka (Fig. 2). Consistently

CPD
9, 3209–3238, 2013

more negative values are reached in both reconstructed $\delta^{18}O_{sw}$ and $\delta D_{alkenone}$ during early MIS5e at about 128 ka. Higher salinity conditions are also observed throughout MIS3/MIS2 in reconstructed $\delta^{18}O_{sw}$ and $\delta D_{alkenone}$ (Fig. 3) followed by comparable freshening trends starting at the onset of Termination I (~ 18 ka). The offset in the timing of the freshening trends between the different proxies is similar to that observed in the Mg/Ca and $U^{K'}_{37}$ SST records. This might be explained by differences in depth habitat and/or salinity effects on Mg/Ca and consequently the reconstructed $\delta^{18}O_{sw}$ record. Despite the discrepancy in the timing of the freshening events, an overall increase in salinity is recorded in both $\delta^{18}O_{sw}$ and $\delta D_{alkenone}$ values for glacial stages MIS6 and MIS3/5. This is followed by a rapid decrease in salinity throughout the terminations. These fresher conditions prevail during the subsequent interglacial stages.

Absolute salinity estimates are difficult to obtain from the $\delta D_{alkenone}$ due to the uncertainties in both the slope and intercept of the culture calibrations and other variables (Rohling, 2007). However, by estimating relative salinity changes only using the slope of the $\delta D_{alkenone}$–salinity relationship we avoid uncertainties related to the intercept. This provides an added advantage that the slopes for *E. huxleyi* or *G. oceanica* are nearly identical, i.e. 4.8 and 4.2 ‰ $\delta D_{alkenone}$ per salinity unit, respectively (Schouten et al., 2006). Estimations for relative salinity changes from $\delta D_{alkenone}$ result in a freshening trend of approximately 1.7–2 salinity units during the course of Termination I, and about 1.5–1.7 during Termination II. These results are in fairly good agreement with the estimated salinity shift of 1.2–1.5 based on combined Mg/Ca SST estimates and $\delta^{18}O$ of planktonic foraminifera for these time periods (Martinez-Mendez et al., 2010). We therefore strongly support the use of $\delta D_{alkenone}$ as a salinity proxy.

Our results show more saline and cooler conditions throughout glacials MIS6 and MIS2/3, subsequently followed by an abrupt late glacial warming and freshening trend during glacial Termination I and II (Figs. 2 and 3). These findings support previous concepts of reduced Agulhas Leakage during glacials followed by late glacial resumption of Indian–Atlantic transport caused by changes in the wind fields and northward migra-

CPD
9, 3209–3238, 2013

tion of sea ice cover and the subtropical fronts (de Ruijter et al., 1999; Kunz-Pirrung et al., 2002; Peeters et al., 2004).

5 Conclusions

In this study, we analyzed two sediment cores from the Agulhas leakage area covering Termination I and II. We combined TEX_{86}^{H} and $U_{37}^{K'}$ SST reconstructions with a previously reported SST record based on Mg/Ca of the planktonic foraminifera *G. bulloides* (Martinez-Mendez et al., 2010). Comparison of the three independent proxies showed differences in absolute temperature estimates, as well as differences in the magnitude and timing of warming from glacial to interglacial periods. Sea surface temperatures reconstructed from three different proxies indicated relatively low temperature conditions throughout the late glacials MIS6 and MIS2/3 in the Agulhas Leakage area. Further, at the onset of the de-glaciation (Termination I and II) temperatures increase significantly. The difference in absolute temperatures and temperature trends between TEX_{86}^{H}, $U_{37}^{K'}$ and Mg/Ca based SST reconstructions could be a result of differences in depth habitats as well as a possible salinity effect on Mg/Ca. In order to further assess the paleodynamics of the Agulhas Current we coupled the reconstructed SST data with reconstructed relative salinity changes using the $\delta D_{alkenone}$. The $\delta D_{alkenone}$ showed a shift from more positive values to more negative values during Termination I and Termination II suggesting elevated salinities during glacial periods, with subsequent freshening during glacial terminations. Similar trends were also observed based on planktonic foraminifera $\delta^{18}O_{sw}$ reconstructions. Estimated salinity changes, based on $\delta D_{alkenone}$, range from 1.7 to 2 salinity units for Termination I and from 1.5 to 1.7 salinity units for Termination II. This is in fairly good agreement with salinity shifts based on the paired Mg/Ca and $\delta^{18}O$ approach of planktonic foraminifera. Our results therefore identify a more efficient Agulhas leakage and thus increased release of Indian Ocean water to the South Atlantic Ocean during the terminations.

CPD
9, 3209–3238, 2013

Acknowledgements. We acknowledge financial support from The Seventh Framework Programme PEOPLE Work Programme, Grant 238512 (Marie Curie Initial Training Network "GATEWAYS"). The Dutch Organization for Scientific Research (NWO) is acknowledged for funding M. van der Meer (VIDI) and S. Schouten (VICI). S. K. would like to thank C. A. Grove (Royal NIOZ, the Netherlands) and D. Chivall (Royal NIOZ, the Netherlands) for their input to this manuscript.

References

Arbuszewski, J., deMenocal, P., Kaplan, A., and Farmer, E. C.: On the fidelity of shell-derived $\delta^{18}O_{sw}$ estimates, Earth Planet. Sci. Lett., 300, 185–196, 2010.

Bard, E.: Comparison of alkenone estimates with other paleotemperature proxies, Geochem. Geophy. Geosy., 2, doi:10.1029/2000gc000050, 2001.

Bard, E. and Rickaby, R. E. M.: Migration of the subtropical front as a modulator of glacial climate, Nature, 460, 380–393, 2009.

Bertrand, P.: Les rapport de campagne a la mer a bord du Marion Dufresne – Campagne NAUSICAA – Images II – MD105 du 20/10/96 au 25/11/96, Plouzane, Inst. Fr. pour la Rech. et la Technol. Polaires, Plouzané, France, 1997.

Biastoch, A., Boning, C. W., and Lutjeharms, J. R. E.: Agulhas leakage dynamics affects decadal variability in Atlantic overturning circulation, Nature, 456, 489–492, 2008.

Bidigare, R. R., Fluegge, A., Freeman, K. H., Hanson, K. L., Hayes, J. M., Hollander, D., Jasper, J. P., King, L. L., Laws, E. A., Milder, J., Millero, F. J., Pancost, R., Popp, B. N., Steinberg, P. A., and Wakeham, S. G.: Consistent fractionation of ^{13}C in nature and in the laboratory: growth-rate effects in some haptophyte algae, Global Biogeochem. Cy., 11, 279–292, 1997.

Curry, W. B. and Crowley, T. J.: The $\delta^{13}C$ of equatorial Atlantic surface waters: implications for Ice Age pCO_2 levels, Paleoceanography, 2, 489–517, 1987.

de Ruijter, W. P. M., Biastoch, A., Drijfhout, S. S., Lutjeharms, J. R. E., Matano, R. P., Pichevin, T., van Leeuwen, P. J., and Weijer, W.: Indian-Atlantic interocean exchange: dynamics, estimation and impact, J. Geophys. Res.-Oceans, 104, 20885–20910, 1999.

dos Santos, R. A. L., Prange, M., Castaneda, I. S., Schefuss, E., Mulitza, S., Schulz, M., Niedermeyer, E. M., Damste, J. S. S., and Schouten, S.: Glacial-interglacial variability in Atlantic

CPD
9, 3209–3238, 2013

meridional overturning circulation and thermocline adjustments in the tropical North Atlantic, Earth Planet. Sci. Lett., 300, 407–414, 2010.
Fallet, U., Ullgren, J. E., Castañeda, I. S., van Aken, H. M., Schouten, S., Ridderinkhof, H., and Brummer, G.-J. A.: Contrasting variability in foraminiferal and organic paleotemperature proxies in sedimenting particles of the Mozambique Channel (SW Indian Ocean), Geochim. Cosmochim. Ac., 75, 5834–5848, 2011.
Ferguson, J. E., Henderson, G. M., Kucera, M., and Rickaby, R. E. M.: Systematic change of foraminiferal Mg/Ca ratios across a strong salinity gradient, Earth Planet. Sci. Lett., 265, 153–166, 2008.
Flores, J. A., Gersonde, R., and Sierro, F. J.: Pleistocene fluctuations in the Agulhas current retroflection based on the calcareous plankton record, Mar. Micropaleontol., 37, 1–22, 1999.
Franzese, A. M., Hemming, S. R., Goldstein, S. L., and Anderson, R. F.: Reduced Agulhas leakage during the Last Glacial Maximum inferred from an integrated provenance and flux study, Earth Planet. Sci. Lett., 250, 72–88, 2006.
Giraudeau, J., Balut, Y., Hall, I. R., Mazaud, A., and Zahn, R.: SWAF-MDI128 Scientific Report, Rep. OCE/2003/01, Inst. Polaire Fr., Plouzane, France, 108 pp., 2003.
Haarsma, R. J., Campos, E. J. D., Drijfhout, S., Hazeleger, W., and Severijns, C.: Impacts of interruption of the Agulhas leakage on the tropical Atlantic in coupled ocean–atmosphere simulations, Clim. Dynam., 36, 989–1003, 2011.
Herndl, G. J., Reinthaler, T., Teira, E., van Aken, H., Veth, C., Pernthaler, A., and Pernthaler, J.: Contribution of Archaea to total prokaryotic production in the deep Atlantic Ocean, Appl. Environ. Microb., 71, 2303–2309, 2005.
Huguet, C., Martrat, B., Grimalt, J. O., Damste, J. S. S., and Schouten, S.: Coherent millennial-scale patterns in $U^{K'}_{37}$ and TEX^{H}_{86} temperature records during the penultimate interglacial-to-glacial cycle in the western Mediterranean, Paleoceanography, 26, Pa2218, doi:10.1029/2010pa002048, 2011.
Karner, M. B., DeLong, E. F., and Karl, D. M.: Archaeal dominance in the mesopelagic zone of the Pacific Ocean, Nature, 409, 507–510, 2001.
Kim, J. H., Schouten, S., Hopmans, E. C., Donner, B., and Damste, J. S. S.: Global sediment core-top calibration of the TEX86 paleothermometer in the ocean, Geochim. Cosmochim. Ac., 72, 1154–1173, 2008.
Kim, J. H., van der Meer, J., Schouten, S., Helmke, P., Willmott, V., Sangiorgi, F., Koc, N., Hopmans, E. C., and Damste, J. S. S.: New indices and calibrations derived from the distribution

CPD
9, 3209–3238, 2013

of crenarchaeal isoprenoid tetraether lipids: implications for past sea surface temperature reconstructions, Geochim. Cosmochim. Ac., 74, 4639–4654, 2010.
Kunz-Pirrung, M., Gersonde, R., and Hodell, D. A.: Mid-Brunhes century-scale diatom sea surface temperature and sea ice records from the Atlantic sector of the Southern Ocean (ODP Leg 177, sites 1093: 1094 and core PS2089-2), Palaeogeogr. Palaeocl., 182, 305–328, 2002.
Lee, K. E., Kim, J.-H., Wilke, I., Helmke, P., and Schouten, S.: A study of the alkenone, TEX86, and planktonic foraminifera in the Benguela Upwelling System: implications for past sea surface temperature estimates, Geochem. Geophy. Geosy., 9, Q10019, doi:10.1029/2008gc002056, 2008.
Locarnini, R. A., Mishonov, A. V., Antonov, J. I., Boyer, T. P., Garcia, H. E., Baranova, O. K., Zweng, M. M., and Johnson, D. R.: World Ocean Atlas 2009, Vol. 1: Temperature, edited by: Levitus, S., NOAA Atlas NESDIS 68, US Government Printing Office, Washington, D.C., 1, 184 pp., 2010.
Lutjeharms, J. R. E.: The Agulhas Current, Springer, Berlin, 2006.
Martinez-Mendez, G., Zahn, R., Hall, I. R., Pena, L. D., and Cacho, I.: 345 000-year-long multi-proxy records off South Africa document variable contributions of northern versus southern component water to the deep South Atlantic, Earth Planet. Sci. Lett., 267, 309–321, 2008.
Martinez-Mendez, G., Zahn, R., Hall, I. R., Peeters, F. J. C., Pena, L. D., Cacho, I., and Negre, C.: Contrasting multiproxy reconstructions of surface ocean hydrography in the Agulhas Corridor and implications for the Agulhas leakage during the last 345 000 years, Paleoceanography, 25, Pa4227, doi:10.1029/2009pa001879, 2010.
Mashiotta, T. A., Lea, D. W., and Spero, H. J.: Glacial–interglacial changes in Subantarctic sea surface temperature and δ^{18}O-water using foraminiferal Mg, Earth Planet. Sci. Lett., 170, 417–432, 1999.
Müller, P. J., Kirst, G., Ruhland, G., von Storch, I., and Rosell-Melé, A.: Calibration of the alkenone paleotemperature index $U^{K'}_{37}$ based on core-tops from the eastern South Atlantic and the global ocean (60° N–60° S), Geochim. Cosmochim. Ac., 62, 1757–1772, 1998.
Niebler, H. S., Hubberten, H. W., and Gersonde, R.: Oxygen isotope values of planktic foraminifera: a tool for the reconstruction of surface water stratification, in: Use of Proxies in Paleoceanography, edited by: Fischer, G. and Wefer, G., Springer, Berlin, Heidelberg, 165–189, 1999.

CPD
9, 3209–3238, 2013

Peeters, F. J. C., Acheson, R., Brummer, G. J. A., de Ruijter, W. P. M., Schneider, R. R., Ganssen, G. M., Ufkes, E., and Kroon, D.: Vigorous exchange between the Indian and Atlantic oceans at the end of the past five glacial periods, Nature, 430, 661–665, 2004.

Penven, P., Lutjeharms, J. R. E., and Florenchie, P.: Madagascar: a pacemaker for the Agulhas Current system?, Geophys. Res. Lett., 33, L17609, doi:10.1029/2006gl026854, 2006.

Prahl, F. G. and Wakeham, S. G.: Calibration of unsaturation patterns in long-chain ketone compositions for paleotemperature assessment, Nature, 330, 367–369, 1987.

Rau, A. J., Rogers, J., Lutjeharms, J. R. E., Giraudeau, J., Lee-Thorp, J. A., Chen, M. T., and Waelbroeck, C.: A 450-kyr record of hydrological conditions on the western Agulhas bank slope, south of Africa, Mar. Geol., 180, 183–201, 2002.

Rau, G. H., Riebesell, U., and WolfGladrow, D.: A model of photosynthetic ^{13}C fractionation by marine phytoplankton based on diffusive molecular CO_2 uptake, Mar. Ecol.-Prog. Ser., 133, 275–285, 1996.

Rohling, E. J.: Paleosalinity: confidence limits and future applications, Mar. Geol., 163, 1–11, 2000.

Rohling, E. J.: Progress in paleosalinity: overview and presentation of a new approach, Paleoceanography, 22, PA3215, doi:10.1029/2007pa001437, 2007.

Rohling, E. J. and Bigg, G. R.: Paleosalinity and $\delta^{18}O$: a critical assessment, J. Geophys. Res.-Oceans, 103, 1307–1318, 1998.

Rouault, M., Penven, P., and Pohl, B.: Warming in the Agulhas Current system since the 1980s, Geophys. Res. Lett., 36, L12602, doi:10.1029/2009gl037987, 2009.

Saher, M. H., Rostek, F., Jung, S. J. A., Bard, E., Schneider, R. R., Greaves, M., Ganssen, G. M., Elderfield, H., and Kroon, D.: Western Arabian Sea SST during the penultimate interglacial: a comparison of $U^{K'}_{37}$ and Mg/Ca paleothermometry, Paleoceanography, 24, PA2212, doi:10.1029/2007pa001557, 2009.

Schneider, R. R., Muller, P. J., and Ruhland, G.: Late Quaternary surface circulation in the east equatorial South Atlantic: evidence from alkenone sea surface temperatures, Paleoceanography, 10, 197–219, 1995.

Schouten, S., Hopmans, E. C., Schefuß, E., and Sinninghe Damsté, J. S.: Distributional variations in marine crenarchaeotal membrane lipids: a new tool for reconstructing ancient sea water temperatures?, Earth Planet. Sci. Lett., 204, 265–274, 2002.

Schouten, S., Ossebaar, J., Schreiber, K., Kienhuis, M. V. M., Langer, G., Benthien, A., and Bijma, J.: The effect of temperature, salinity and growth rate on the stable hydrogen iso-

CPD
9, 3209–3238, 2013

topic composition of long chain alkenones produced by *Emiliania huxleyi* and *Gephyrocapsa oceanica*, Biogeosciences, 3, 113–119, doi:10.5194/bg-3-113-2006, 2006.
Schouten, S., Huguet, C., Hopmans, E. C., Kienhuis, M. V. M., and Sinninghe Damsté, J. S.: Analytical methodology for TEX_{86} paleothermometry by high-performance liquid chromatography/atmospheric pressure chemical ionization-mass spectrometry, Anal. Chem., 79, 2940–2944, 2007.
Srivastava, R., Ramesh, R., Jani, R. A., Anilkumar, N., and Sudhakar, M.: Stable oxygen, hydrogen isotope ratios and salinity variations of the surface Southern Indian Ocean waters, Curr. Sci. India, 99, 1395–1399, 2010.
van der Meer, M. T. J., Baas, M., Rijpstra, W. I. C., Marino, G., Rohling, E. J., Sinninghe Damsté, J. S., and Schouten, S.: Hydrogen isotopic compositions of long-chain alkenones record freshwater flooding of the Eastern Mediterranean at the onset of sapropel deposition, Earth Planet. Sci. Lett., 262, 594–600, 2007.
van der Meer, M. T. J., Sangiorgi, F., Baas, M., Brinkhuis, H., Sinninghe Damsté, J. S., and Schouten, S.: Molecular isotopic and dinoflagellate evidence for Late Holocene freshening of the Black Sea, Earth Planet. Sci. Lett., 267, 426–434, 2008.
van der Meer, M. T. J., Benthien, A., Bijma, J., Schouten, S., and Sinninghe Damsté, J. S.: Alkenone distribution impacts the hydrogen isotopic composition of the $C_{37:2}$ and $C_{37:3}$ alkan-2-ones in *Emiliania huxleyi*, Geochim. Cosmochim. Ac., doi:10.1016/j.gca.2012.10.041, 2013.
van Sebille, E., Biastoch, A., van Leeuwen, P. J., and de Ruijter, W. P. M.: A weaker Agulhas Current leads to more Agulhas leakage, Geophys. Res. Lett., 36, L03601, doi:10.1029/2008gl036614, 2009.
van Sebille, E., Beal, L. M., and Johns, W. E.: Advective time scales of Agulhas leakage to the North Atlantic in surface drifter observations and the 3-D OFES model, J. Phys. Oceanogr., 41, 1026–1034, 2011.
Waelbroeck, C., Labeyrie, L., Michel, E., Duplessy, J. C., McManus, J. F., Lambeck, K., Balbon, E., and Labracherie, M.: Sea-level and deep water temperature changes derived from benthic foraminifera isotopic records, Quaternary Sci. Rev., 21, 295–305, 2002.
Weeks, S. J., Shillington, F. A., and Brundrit, G. B.: Seasonal and spatial SST variability in the Agulhas retroflection and Agulhas return current, Deep-Sea Res. Part I, 45, 1611–1625, 1998.

CPD
9, 3209–3238, 2013

Wuchter, C., Schouten, S., Wakeham, S. G., and Sinninghe Damsté, J. S.: Archaeal tetraether membrane lipid fluxes in the northeastern Pacific and the Arabian Sea: implications for TEX_{86} paleothermometry, Paleoceanography, 21, PA4208, doi:10.1029/2006pa001279, 2006.

CPD
9, 3209–3238, 2013

Table 1. Results for combined $C_{37:2-3}$ alkenone stable hydrogen isotope ($\delta D_{alkenone}$, ‰), stable carbon isotope ($\delta^{13}C_{alkenone}$), TEX_{86}^{H} values (Kim et al., 2010) and $U_{37}^{K'}$ values (Prahl and Wakeham, 1987) for core MD96-2080.

Age (ka)	$U_{37}^{K'}$	TEX_{86}^{H}	$\delta D_{alkenone}$* (‰)	$\delta^{13}C_{alkenone}$* (‰)
117.7	0.819	−0.276	−197 ± 2	
119.9	0.819	−0.272	−196 ± 2	
123.1	0.856	−0.277	−180	
125.4	0.864	−0.278	−193 ± 4	−24.7 ± 0.5
126.5	0.833	−0.273	−194 ± 1	−25.4 ± 0.2
127.0	0.829	−0.274	−198 ± 0	
127.9	0.845	−0.275	−188 ± 1	−25.1 ± 0.8
128.7	0.851	−0.266	−194 ± 4	−25.6 ± 0.4
129.8	0.828	−0.248	−194 ± 0	
131.3	0.821	−0.253	−192 ± 3	
132.8	0.798	−0.250	−189 ± 2	−24.2 ± 0.4
133.6	0.819	−0.238	−190 ± 0	−23.9 ± 0.1
135.1	0.776	−0.235	−182 ± 2	
137.3	0.750	−0.251	−182 ± 4	−24.5 ± 0.1
137.7	0.749	−0.256	−183 ± 1	−24.1 ± 0.4
141.2	0.709	−0.321	−179 ± 1	
142.2	0.710	−0.320	−177 ± 3	
145.0	0.717	−0.325	−180 ± 1	−24.9 ± 0.1
147.5	0.726	−0.309		
151.5	0.707	−0.314	−184 ± 2	−24.8 ± 0.6
152.0	0.734	−0.314	−182 ± 0	
154.7	0.724	−0.330	−186 ± 1	−24.6 ± 0.2
158.0	0.738	−0.290	−177 ± 0	
162.3	0.745	−0.332	−179 ± 3	
168.8	0.745	−0.314	−191 ± 2	
177.9	0.714	−0.292	−190 ± 3	
182.7	0.707	−0.303	−187 ± 3	

* The error is defined as the range of duplicated measurements.

CPD
9, 3209–3238, 2013

Table 2. Results for combined $C_{37:2-3}$ alkenone stable hydrogen isotope ($\delta D_{alkenone}$, ‰), stable carbon isotope ($\delta^{13}C_{alkenone}$), TEX_{86}^{H} values (Kim et al., 2010) and $U_{37}^{K'}$ values (Prahl and Wakeham, 1987) for core MD02-2594.

Age (ka)	$U_{37}^{K'}$	TEX_{86}^{H}	$\delta D_{alkenone}$ * (‰)	$\delta^{13}C_{alkenone}$ * (‰)
3.5	0.724	−0.305	−192 ± 2	−24.1 ± 0.1
5.6	0.723	−0.307	−184 ± 2	
6.3	0.746	−0.309	−189 ± 4	
6.9	0.736	−0.311	−182 ± 1	
8.6	0.753	−0.308	−191 ± 3	
12.0	0.762	−0.282	−178 ± 2	−24.1 ± 0.8
18.0	0.685	−0.308	−179 ± 1	
18.5	0.677	−0.366	−171 ± 2	
21.1	0.672	−0.336	−173 ± 3	−24.2 ± 1.1
22.3	0.686	−0.352	−178 ± 2	
26.7	0.686	−0.328	−166 ± 2	
28.4	0.682	−0.333	−173 ± 0	
29.5	0.686	−0.339	−172 ± 1	
30.8	0.715	−0.313	−179 ± 2	
31.5	0.692	−0.332	−173 ± 2	−23.6 ± 0.1
32.0	0.696	−0.315	−177 ± 1	
37.4	0.728	−0.312	−171 ± 3	
42.1	0.676	−0.343	−180 ± 2	

* The error is defined as the range of duplicated measurements.

CPD
9, 3209–3238, 2013

Table 3. Average values for the hydrogen isotope composition of the $C_{37:2-3}$ alkenones, the global $\delta^{18}O_{ice\ vol.}$ (Waelbroeck et al., 2002), $\delta D_{ice\ vol.}$ (Srivastava et al., 2010) and the local δD_{sw} derived from $\delta^{18}O$ of *G. bulloides* (Martinez-Mendez et al., 2011) for the intervals of before and after Termination I and II.

	Time interval	$\delta D_{alkenone}$ (‰)	$\delta^{18}O_{ice\ vol.}$ (‰)	$\delta D_{ice\ vol.}$ (‰)	δD_{sw} (‰)
TI	3.5–8.6 ka (n = 5)	−188	0.06	0.72	−0.41
	18–37.4 ka (n = 11)	−174	0.83	6.34	6.53
TII	117.7–129.8 ka (n = 9)	−194	0.00	0.30	−0.51
	141.2–162.3 ka (n = 8)	−180	0.88	6.71	9.63

CPD
9, 3209–3238, 2013

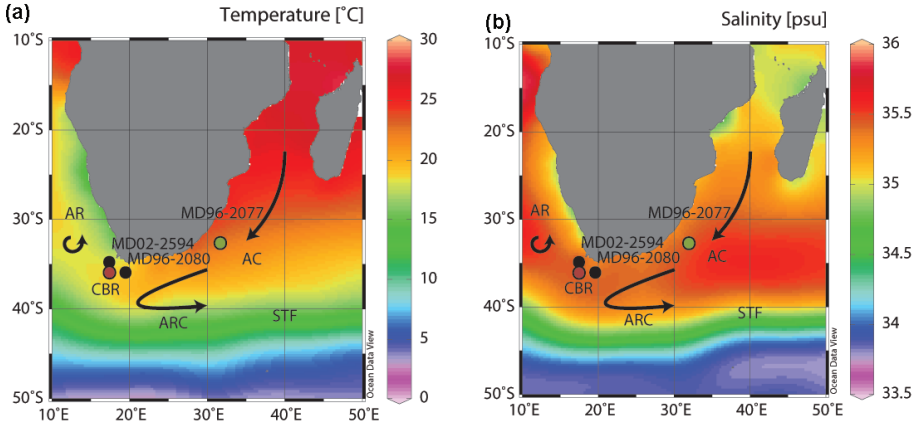

Fig. 1. Location of the cores MD02-2594 and MD96-2080 (black dots) and reference sites Cape Basin record (CBR, red dot) (Peeters et al., 2004), MD96-2077 (green dot) (Bard and Rickaby 2009) and oceanographic setting on **(a)** a map of modern sea surface temperatures and **(b)** a map of modern sea surface salinity. Agulhas Current (AC), Agulhas Return Current (ARC), Agulhas rings (AR), Subtropical Front (STF) and Sub Antarctic Front (SAF). The underlying maps of modern sea surface temperatures and salinity were compiled with high resolution CTD data from http://www.nodc.noaa.gov and the Ocean Data View software version 4.3.7 by Schlitzer, R., Ocean Data View (http://odv.awi.de), 2010.

CPD
9, 3209–3238, 2013

CC BY

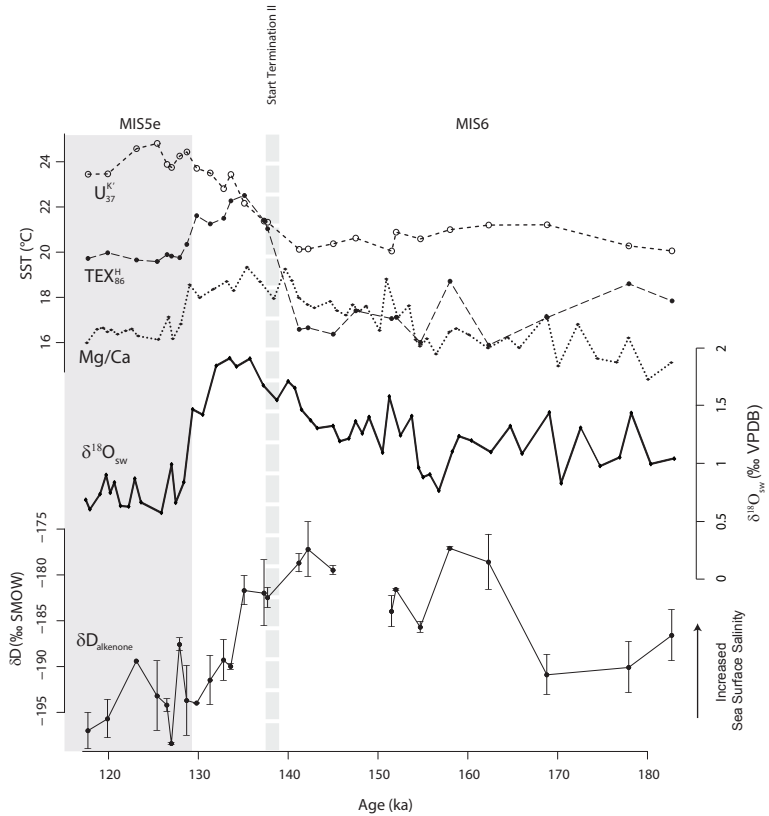

Fig. 2. Reconstructed SST of $U^{K'}_{37}$ (dashed line, open circles), TEX^{H}_{86} (dashed line, closed circles), Mg/Ca of *G. bulloides* (dotted line, closed circles, Martinez-Mendez et al., 2010), reconstructed $\delta^{18}O_{sw}$ from *G. bulloides* (solid line, diamonds, Martinez-Mendez et al., 2010) and hydrogen isotope composition of $C_{37:2-3}$ alkenones (solid line, closed circles) for core MD96-2080.

CPD
9, 3209–3238, 2013

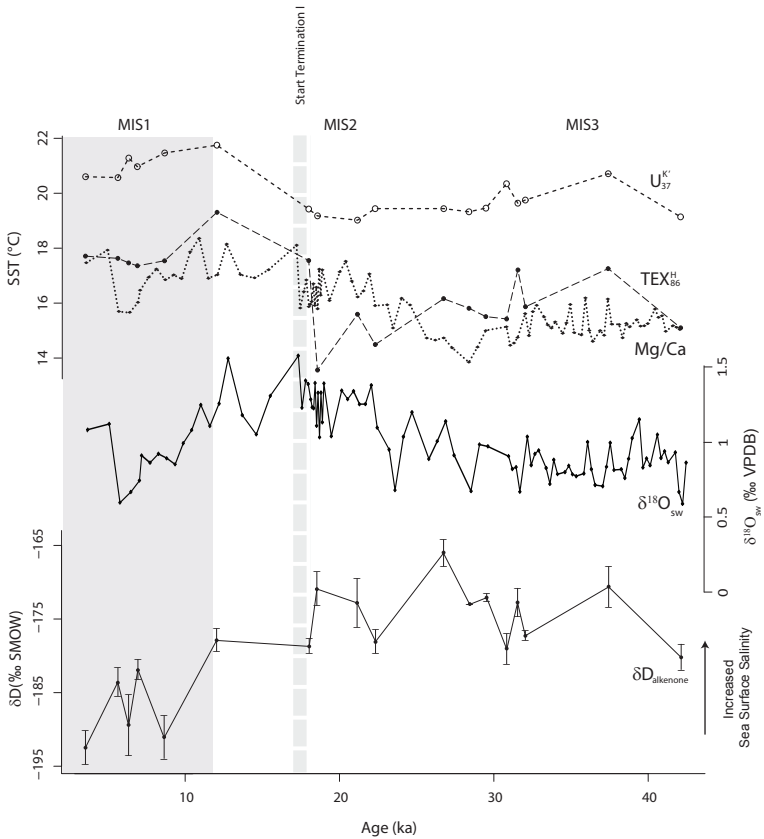

Fig. 3. Reconstructed SST of $U^{K'}_{37}$ (dashed line, open circles), TEX^{H}_{86} (dashed line, closed circles), Mg/Ca of *G. bulloides* (dotted line, closed circles, Martinez-Mendez et al., 2010), reconstructed $\delta^{18}O_{sw}$ from *G. bulloides* (solid line, diamonds, Martinez-Mendez et al., 2010) and hydrogen isotope composition of $C_{37:2-3}$ alkenones (solid line, closed circles) for core MD02-2594.

CPD
9, 3209–3238, 2013

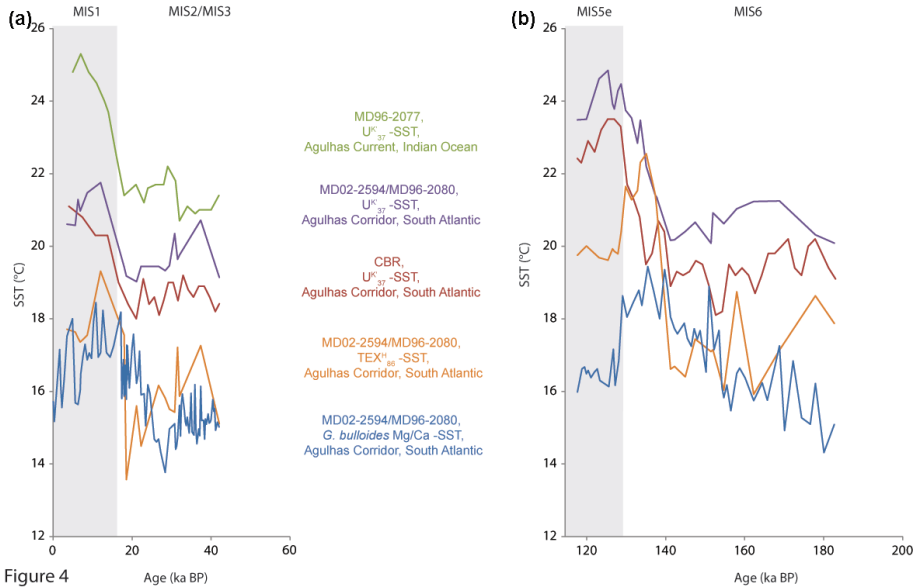

Figure 4

Fig. 4. Comparison of $U^{K'}_{37}$ SST, TEX^{H}_{86} SST and *G. bulloides* Mg/Ca SST (Martinez-Mendez et al., 2010) of **(a)** core MD02-2594 and **(b)** core MD96-2080 (see Fig. 1 for core location) with $U^{K'}_{37}$ SST of MD96-2077 in the Agulhas Current, Indian Ocean (Bard and Rickaby 2009) and $U^{K'}_{37}$ SST of CBR in the Agulhas Corridor, South Atlantic (Peeters et al., 2004).

CPD
9, 3209–3238, 2013